Electronic energy transfer on a vibronically coupled quantum aggregate

Jan Roden,[1,a)] Georg Schulz,[2,b)] Alexander Eisfeld,[1,c)] and John Briggs[1,2,d)]
[1]*Max Planck Institute for the Physics of Complex Systems, Nöthnitzer Str. 38, 01187 Dresden, Germany*
[2]*Theoretical Quantum Dynamics, Physics Institute, University of Freiburg, Hermann-Herder-Str. 3, 79104 Freiburg, Germany*

(Received 7 May 2009; accepted 23 June 2009; published online 30 July 2009)

We examine the transfer of electronic excitation (an exciton) along a chain of electronically coupled monomers possessing internal vibronic structure and which also interact with degrees of freedom of the surrounding environment. Using a combination of analytical and numerical methods, we calculate the time evolution operator or time-dependent Green's function of the system and thereby isolate the physical parameters influencing the electronic excitation transport. Quite generally, we show that coupling to vibrations slows down and inhibits migration of electronic excitation due to dephasing effects on the coherent transfer present without vibrations. In particular, coupling to a continuous spectrum of environment states leads to a complete halting of transfer, i.e., a trapping of the exciton. © *2009 American Institute of Physics*. [DOI: 10.1063/1.3176513]

I. INTRODUCTION

The problem of the time dependence and character of electronic excitation transport (EET) along aggregates of atoms, molecules, or other monomeric quantum objects is enjoying renewed interest in the light of refined experimental, device fabrication, and molecular manipulation techniques. Apart from traditional quantum aggregates, such as those composed of organic molecules, e.g., crystals,[1–4] dendrimers,[5] *J*-aggregates,[6] photosynthetic units,[7–11] new types of aggregate, such as cold atom[12–14] or quantum dot assemblies,[15] mixed aggregates of metal nanoparticles, and organic molecules,[16] are being studied. New, more sophisticated probing and detection techniques allow studies on EET with increasing spatial and temporal resolutions. In some cases, the nature of EET on such aggregates is considered to be due to the quantum coherence embodied in the very concept of the delocalized exciton. This coherence is affected strongly by the interaction with the "environment," usually in the form of nuclear vibrations, and hence such interactions, leading to decoherence, alter the nature and probability of migration of electronic excitation along the aggregate.

In this paper we will concentrate on the molecular Frenkel exciton problem, considering molecular aggregates composed of monomers whose absorption bands show broad vibrational structure. Since the molecules in weakly bound aggregates largely retain their character, we will use the language of molecular rather than solid-state physics. In a molecular aggregate, usually studied in solution, the electronic excitation interacts with various types of vibration, as classified in Ref. 17. First and foremost, there are the intramolecular vibrational excitations directly accompanying light absorption due to a shift of the equilibrium position of the nuclei on electronic excitation. These primary intramolecular vibrations we call internal modes (IMs). They are evident in the absorption spectra of isolated monomers and usually dominated by one or a few normal modes. At low temperatures, these modes can clearly be seen.[18] In large organic molecules, these primary vibrations couple to many other IMs so that the absorption spectrum consists of many vibronic lines. In solution, the intramolecular vibrations interact with a myriad of lower frequency modes (arising from the increase in the mass of the vibrators) representing phonons on the aggregate itself or vibrational, rotational, and translational degrees of freedom of the surrounding liquid molecules. We will call such external modes, specified usually only by a continuous mode density, EMs. In addition, there is a broadening due to local variations in the electronic interaction of a given monomer with the surrounding molecules.

The objective of this paper is to study the propagation of an initially localized electronic excitation along a molecular aggregate, interacting with both IM and EM vibrations. The relevant time scales are then (a) the typical time T_{el} for transfer of electronic excitation due to intermonomer coupling and (b) the typical time T_{vib} for the onset of electronic-vibrational coupling. In the energy picture these times correspond to the half-width $B=\hbar/T_{\mathrm{el}}$ of the exciton band and the width $\sigma=\hbar/T_{\mathrm{vib}}$ of the monomer vibronic absorption spectrum.

In the specific case of molecular aggregates, this EET problem has been tackled using two rather distinct sets of approximation to the full problem, which lead to two different pictures of the transfer process.

(1) On the one hand, and by far the most popular approach, the intramolecular vibrations are not considered explicitly and interest is centered on the influence of coupling to the surroundings. This follows the methods of solid-state physics and usually the language is that of second quantization and linear exciton-phonon coupling. In the zeroth order, an aggregate is taken to consist of mono-

[a)]Electronic mail: roden@mpipks-dresden.mpg.de.
[b)]Electronic mail: Georg.Schulz@unibas.ch.
[c)]Electronic mail: eisfeld@mpipks-dresden.mpg.de.
[d)]Electronic mail: john.briggs@physik.uni-freiburg.de.

mers with only a single sharp electronic transition line. Due to coupling to the surrounding, each monomer at a different site along the aggregate is subject to fluctuating forces, which leads to a change in the effective electronic transition energy and/or in the strength of electronic coupling to neighboring monomers. The shifts and coupling changes are then treated statistically according to some prescription. A distinction between IM and EM is not made usually, all being treated simply as phonons. Indeed, often the precise origin of monomer transition energy fluctuations, whether from changed electronic interaction with fluctuating surroundings, from local inhomogeneities, or from interaction with vibrations, rotations, or translations of the environment, need not be specified. Rather, those fluctuations are treated as distributions whose character can be assumed and whose effect can be described via fit parameters to explain the experimental data. This disorder model has been applied extensively in the energy domain (as examples see Refs. 19–22), beginning with the works of Schreiber and Toyozawa[19] and Knapp.[23] The main effect of disorder in the transition energies is to localize the otherwise delocalized purely electronic excitonic wave functions. This effect is illustrated clearly in the works of Malyshev and co-workers.[24–26] When transfer in the time domain is considered in this model, the varying excitation energy barriers between monomers lead to trapping of excitation in these localized regions. Finite temperature may provoke a jumping over these barriers and renewed transport.[27,28] The final picture is one of hopping between these localized regions with essential destruction of coherent exciton transfer except within the limited domains of the localized wave functions.

(2) On the other hand, which is the approach of the present paper, one uses the molecular language of wave functions and Green's functions built from them. First one recognizes that all organic molecules possess rich internal vibrational structure. Then one must take the intramolecular IM modes of identical monomers explicitly into account. Transitions into and out of the electronically excited state as the exciton propagates are accompanied by transitions, weighed by Franck–Condon (FC) factors, into and out of vibrational states. This leads to an effective dilution of the electronic coupling and effective variations in the transition energies. The influence of the surroundings is then taken into account by considering their vibrational states to be continuously distributed, corresponding to coupling to an open system, and leading to a continuous absorption spectrum. Now there is essentially a continuous distribution of vertical transition energies and a continuous distribution of electronic monomer-monomer coupling strengths via the continuous FC factor. Hence the picture of transport which emerges is much more complicated than that of pure electronic excitation transfer.

The monomer models appropriate to the method described in (2) are illustrated in the sketch of Fig. 1. We consider a ground-state Born–Oppenheimer (BO) potential well. When the monomer absorption spectrum exhibits some discrete IM structure, the left figure (a) is applicable, in which absorption is to discrete states of the upper BO potential. A popular simplification is to take the ground and upper BO potentials to be of the same harmonic form, giving vibrational spacing $\hbar\omega$ but with the minimum of the upper potential shifted by an amount $\bar{Q}$ from that of the ground state. Then the FC factors can be expressed in a closed form. For example, when absorption is from the lowest state of the ground BO potential to vibrational states α of the upper potential, one has the FC factor f_0^α with

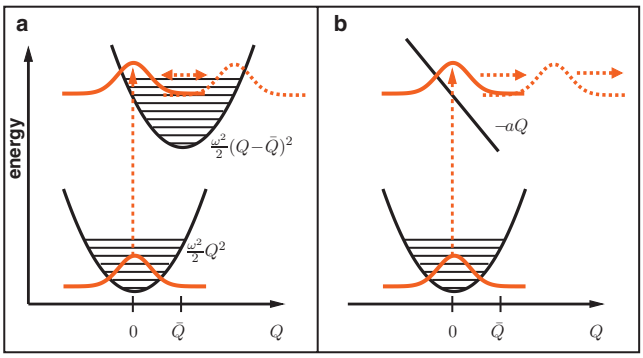

FIG. 1. Sketch of the lower and upper monomer BO potential curves: (a) with discrete levels in the upper potential (reflected wavepacket) and (b) with a continuum (outgoing wavepacket).

$$|f_0^\alpha|^2 = \frac{X^\alpha}{\alpha!}\exp(-X), \tag{1}$$

i.e., a Poisson distribution of FC factors. Here X is the dimensionless Huang–Rhys factor $X=\omega\bar{Q}^2/2\hbar$.[29] In this case the absorption band has width (standard deviation) $\sigma=\sqrt{X}$ in units of the vibrational energy quantum $\hbar\omega$.

Clearly the establishment of discrete vibronic structure requires multiple reflections of the wavepacket on the upper potential, as illustrated schematically in Fig. 1(a). Interaction with EM corresponds to suppression of 100% reflection at the outer turning point and a broadening of the vibronic line. The limit of continuous broadening is mimicked by effectively moving the outer turning point to infinity, giving a purely outgoing vibrational wavepacket. Then, in the region of FC overlap, the upper potential can be modeled by a linear potential, as sketched in Fig. 1(b). As shown in Appendix B (see also Refs. 30 and 31), this gives rise to a single continuous monomer absorption peak. Also this procedure corresponds to taking a particular limit of the discrete spectrum in Fig. 1(a). This limit is $X\to\infty, \omega\to 0$ in the upper electronic potential such that the spectral width $\sqrt{X}\hbar\omega$ remains constant. This will be used later in numerical work to represent a continuously broadened absorption spectrum.

We have applied extensively the approach described in (2) in the energy domain mainly to calculate aggregate absorption spectra.[32–37] However, the theory, which uses an energy-dependent Green's function approach, could also be used to estimate the range of propagation of excitons of given energy interacting with a continuous distribution of vibrational modes.[32,33] The results showed a clear curtail-

ment of exciton propagation length depending on the strength of the vibronic coupling compared to the electronic monomer-monomer coupling. Here we return to this problem but treat it explicitly in the time domain by the use of the time-dependent Green's function (time propagator) for the vibronically coupled aggregate including both discrete IM vibrations and continuous environment EM.

The plan of the paper is as follows. In Sec. II we define the vibronic Hamiltonian of the aggregate and introduce the time-dependent and time-independent Green's operators (propagators) of both monomer and aggregate. The main aim of the paper is to examine first the influence of IM alone on EET and then to extend consideration to the additional coupling to a broad continuum of EM. In this way we isolate the effects of discrete and continuous modes. However, the explicit effect of energy dissipation due to coupling with the surroundings and the related effect of changing temperature will largely not be taken into account. That is, we will assume that the vibrational state of an excited molecule is not changed due to vibrational interaction but only due to electronic interaction.

In this paper, strong and weak couplings will be defined according to the criterion introduced by Simpson and Peterson[38] as the ratio between the exciton band half-width B and the width σ of the monomer absorption spectrum. This dimensionless Simpson–Peterson (SP) parameter will be called $\mathrm{SP}=B/\sigma=T_{\mathrm{vib}}/T_{\mathrm{el}}$. Strong coupling occurs when this value is much greater than unity and weak coupling when much less than unity. All other cases are designated as intermediate coupling.

In Sec. III we consider an exciton on a one-dimensional aggregate coupled to a single IM mode of the monomers. First, the problem is treated exactly in that the full aggregate vibronic Hamiltonian is represented by expansion in a suitable set of vibronic basis states, chosen large enough to ensure convergence. Then the time-dependent Schrödinger equation is solved by propagation numerically in time. This allows calculation of the probability $P_{n0}(t)$ that electronic excitation, initially localized on monomer zero, has arrived at monomer n at time t. Due to limits on computer storage, the exact calculations are restricted to rather short aggregates. However, we also calculate $P_{n0}(t)$ in the "coherent exciton scattering" (CES) approximation.[32,33] In this approximation, only the ground vibrational state of the ground electronic state is taken into account. With this limitation, calculations are possible for very large aggregates. In Sec. III we show that the CES approximation gives generally good agreement with the exact calculations. Hence in the rest of the paper, the CES approximation is used.

The numerical solution of the time-dependent Schrödinger equation is equivalent to a numerical evaluation of the time-dependent propagator or Green's function. In Sec. IV we show first that in both limits of strong coupling and extreme weak coupling, in the CES approximation the time-dependent Green's function can be evaluated analytically. This yields analytic forms for $P_{n0}(t)$, which are the closed form expressions derived separately by Merrifield[39] and Bierman.[40] Finally in CES approximation, $P_{n0}(t)$ is evaluated numerically for all coupling strengths and for large aggregates, initially for monomers with only one IM discrete mode of internal vibration and then for a more realistic case where continuous EMs are also included. In this latter case we use a fit to a measured continuous monomer absorption spectrum of the pseudoisocyanine (PIC) dye. Inclusion of coupling to EM gives rise to a qualitatively new effect, namely, trapping of the exciton. In Sec. IV D an approximate analytic solution, originally due to Magee and Funabashi,[41] is derived which allows the trapping phenomenon to be explained. A summary of results and our conclusions are given in Sec. V.

II. AGGREGATE HAMILTONIAN AND GREEN'S FUNCTION

In this work, for simplicity, we will restrict discussion to a one-dimensional aggregate consisting of N monomers. The EET along the aggregate will be investigated in two ways. In the numerically exact method, the aggregate state is propagated in time by solving the time-dependent Schrödinger equation

$$i\hbar\partial_t|\Psi(t)\rangle = H|\Psi(t)\rangle, \tag{2}$$

with the total aggregate vibronic Hamiltonian H expressed in the basis of aggregate vibronic states (taking into account enough states to ensure convergence). The solution of this equation is equivalent to solving for the time-dependent propagator, or time-dependent Green's operator,

$$G(t) = \exp(-iHt/\hbar)\Theta(t). \tag{3}$$

In the second method, useful for analytic evaluation, the time-dependent Green's function, i.e., the operator $G(t)$ expressed in a vibronic basis, is obtained in closed form, in strong and weak-coupling limits, by using the CES approximation to the energy-dependent Green's function, followed by a Fourier transform to the time representation.

For very long aggregates, constraints on computer storage oblige us to use an approximation also in the first method when solving the time-dependent Schrödinger equation numerically. The approximation we choose is equivalent to the CES approximation, hence combining the two methods.

We adopt a model of an aggregate composed of monomers with one excited electronic state and one vibrational degree of freedom leading to a single vibrational progression in monomer absorption from the ground state. The lower and upper potential curves can, but do not have to, be harmonic as in the standard approach. Simply we assume that the upper curve minimum is shifted from that of the ground electronic state to a larger distance. The nature of the vibrations is then expressed solely in the discrete or continuous distribution of FC factors describing transitions between vibrational states of the lower and upper manifolds. The monomers are coupled electronically and it is assumed that this coupling is independent of vibrational coordinates. The monomer and aggregate Hamiltonians are identical to those described in detail in Refs. 32, 33, and 35, where the absorption spectra of J- and H-aggregates were presented. The Hamiltonian and Green's operators will be expressed in terms of basis states in which electronic excitation is localized on one monomer, i.e., we define

$$|\pi_n\rangle := |\phi_n^e\rangle \prod_{m\neq n} |\phi_m^g\rangle, \tag{4}$$

where $|\phi_n^g\rangle$ and $|\phi_n^e\rangle$ are the ground and excited electronic states of monomer n, respectively (the monomers are taken to be identical). In this basis, the Green's operator has electronic matrix elements

$$G_{nm}(t) = \langle \pi_n | G(t) | \pi_m \rangle, \tag{5}$$

which are still operators in the space of nuclear coordinates. If the aggregate state at time zero is denoted by $|\Psi(0)\rangle$, the state at later times is given by

$$|\Psi(t)\rangle = G(t)|\Psi(0)\rangle. \tag{6}$$

To consider excitation propagation, we must specify the initial state. The simplest way to study EET is to assume that an arbitrary monomer, let us call it monomer 0, alone is excited at time zero. Since electronic excitation can be considered instantaneous on vibrational time scales, then the appropriate initial aggregate vibrational state is that with all monomers in their respective vibrational ground state, i.e.,

$$|\Psi(0)\rangle = |\pi_0\rangle|\Sigma_g\rangle, \tag{7}$$

where

$$|\Sigma_g\rangle = \prod_m |\xi_m^0\rangle \tag{8}$$

and $|\xi_m^0\rangle$ is the lowest vibrational state of the ground electronic state of monomer m. The vibronic basis states where one monomer is excited electronically are defined as a straightforward generalization of Eqs. (4) and (8), i.e.,

$$|\pi_n\rangle|\{\alpha\}_n\rangle = |\pi_n\rangle|\xi_1^{\alpha_1} \cdots \chi_n^{\alpha_n} \cdots \xi_N^{\alpha_N}\rangle, \tag{9}$$

where $\chi_n^{\alpha_n}$ is the vibrational wave function of the electronically excited monomer n with α_n vibrational quanta and the remaining α_i denotes the vibrational quanta in the ground electronic state of each monomer i. Throughout the work we will use χ to denote vibrational states of an electronically excited monomer and ξ for the vibrational states of a monomer in the electronic ground state.

The probability $P_{n0}(t)$ that the electronic excitation resides on monomer n at time t is given by

$$P_{n0}(t) = \sum_{\{\alpha\}} |\langle \{\alpha\}_n | \langle \pi_n | \Psi(t) \rangle|^2 = \sum_{\{\alpha\}} |\langle \{\alpha\}_n | G_{n0}(t) | \Sigma_g \rangle|^2, \tag{10}$$

where a summation has been made over all possible final vibrational states of the aggregate when monomer n is excited electronically.

Next, for later use, we consider energy-dependent Green's operators from which the time-dependent ones can be calculated by Fourier transformation. For noninteracting monomers we define the energy-dependent Green's operator at energy E as

$$g(E) = (E - H_{\text{mon}} + i\delta)^{-1}, \quad \delta = 0_+, \tag{11}$$

where H_{mon} is the total vibronic Hamiltonian of noninteracting monomers. Denoting the electronic coupling operator between monomers by V, then $H = H_{\text{mon}} + V$ is the total aggregate vibronic Hamiltonian and the energy-dependent aggregate Green's operator is

$$G(E) = (E - H + i\delta)^{-1}. \tag{12}$$

The aggregate Green's operator satisfies the equation

$$G(E) = g(E) + g(E)VG(E). \tag{13}$$

To consider the propagation of electronic excitation in time, we need the time-dependent Green's operators defined by Eq. (3) for the full Hamiltonian and by

$$g(t) = \exp(-iH_{\text{mon}}t/\hbar)\Theta(t) = \frac{i}{2\pi}\int_{-\infty}^{\infty} g(E)e^{-iEt/\hbar}dE \tag{14}$$

for propagation by noninteracting monomers.

In the electronic basis (4), the Dyson equation (13) reads as

$$G_{nm}(E) = g_n(E)\delta_{nm} + g_n(E)\sum_{n'} V_{nn'}G_{n'm}(E). \tag{15}$$

Note that G_{nm} and g_n are still operators in the space of nuclear coordinates. However, we will ignore the nuclear coordinate dependence of the electronic coupling matrix elements $V_{nn'}$ and take them to be constants for fixed intermonomer separation and orientation. Then, in the time domain, Eq. (15) reads as

$$G_{nm}(t) = g_n(t)\delta_{nm} - \frac{i}{\hbar}\int_0^{\infty} g_n(t-t')\sum_{n'} V_{nn'}G_{n'm}(t')dt'. \tag{16}$$

Equations (10), (15), and (16) will be used in the following to discuss the EET process.

III. NUMERICALLY EXACT TIME PROPAGATION: COUPLING TO ONE DISCRETE VIBRATIONAL MODE

In order to solve the time-dependent Schrödinger equation (2) numerically, the aggregate vibronic Hamiltonian and the time-dependent aggregate state $|\Psi(t)\rangle$ will be expressed in a truncated set of the vibronic basis states of Eq. (9). Then the time propagation is calculated straightforwardly using a fourth order Runge–Kutta algorithm. The Hamiltonian matrix elements in this basis are

$$\langle \{\alpha\}_n | \langle \pi_n | H | \pi_m \rangle | \{\beta\}_m \rangle = \epsilon^{\{\alpha\}_n}\delta_{nm}\delta_{\{\alpha\}_n\{\beta\}_m} + V_{nm} f_{\beta_n}^{\alpha_n} (f_{\alpha_m}^{\beta_m})^* \prod_{\substack{i=1 \\ i\neq n,m}}^{N} \delta_{\alpha_i\beta_i}, \tag{17}$$

where $\epsilon^{\{\alpha\}_n}$ is the sum of the monomer electronic excitation energy ϵ_{el} of monomer n and all vibrational quanta in the state $|\pi_n\rangle|\{\alpha\}_n\rangle$. The FC overlap matrix elements are defined as

$$f_{\beta_n}^{\alpha_n} = \langle \chi^{\alpha_n} | \xi^{\beta_n} \rangle, \tag{18}$$

denoting a transition from the state ξ^{β_n} of the lower potential to the state χ^{α_n} in the upper potential curve of monomer n (with * in Eq. (17) we denote the complex conjugate). Then we use Eqs. (2) and (10) to calculate the time-dependent

TABLE I. Relations between quantities used: T_{el} is the typical time for EET, B is the half-width of the exciton band, T_{vib} is the typical time for electronic-vibrational coupling, σ is the width of the monomer vibronic absorption spectrum, SP is the Simpson–Peterson parameter, $V=V_{n,n+1}$ is the nearest-neighbor electronic intermonomer interaction, X is the Huang–Rhys parameter, ω is the vibrational frequency, and $\bar{Q}$ is the shift of the harmonic BO potentials.

$T_{el}=\hbar/B$	$T_{vib}=\hbar/\sigma$	$SP=B/\sigma$
$B=2V$	$\sigma=\sqrt{X}\hbar\omega$	$X=\omega\bar{Q}^2/2\hbar$

probability that a given monomer n is excited electronically.

The dynamics of excitation transfer depend essentially on the dimensionless SP parameter $SP=B/\sigma$. It is the intermonomer electronic coupling that drives the excitation transfer. In nearest-neighbor approximation and neglecting end effects, this is given simply by $B=2V$, where $V=V_{n,n+1}$ is assumed to be independent of n. In this section (although not throughout the paper), we will adopt the standard model of identical harmonic potentials in the ground and excited electronic states. The electronic coupling then is measured in units of $\hbar\omega$, the vibrational quantum. In this model the dimensionless Huang–Rhys parameter X is a direct measure of the strength of intramonomer vibronic coupling. This parameter also decides the energy width $\sigma=\sqrt{X}\hbar\omega$ of the monomer absorption spectrum through the Poissonian distribution of FC factors [Eq. (1)]. Hence the ratio $2V/\sigma$ is the SP parameter value and a measure of the excitonic coupling strength. Also it is meaningful to express time in units of T_{el}, the typical time of intermonomer excitation transfer, given in this case by $(\hbar/2V)$. In Table I the relations between the quantities used in the analysis are summarized.

For short aggregates it is important to note that, for a circular aggregate, interference between counterpropagating wavepackets occurs after the excitation wave travels 180° around the circle. Similarly, for a linear aggregate, reflection at the end points leads to interference with the primary wave. To avoid such effects, here we will concentrate on the short-time behavior, considering the excitation wave rolling out from monomer 0 and showing $P_{n0}(t)$ only up to times where the primary wave front reaches the penultimate monomer. Typical results of full calculations for $P_{n0}(t)$ according to Eq. (10) are presented in Figs. 2–4. The dimension of the basis states of Eq. (9) is given by $D=Nn_e n_g^{N-1}$, where n_e is the number of vibrational states included for the excited electronic state and n_g is for the ground electronic state. For this reason, for fixed N and n_e, the values of n_g must be rather limited to make the problem numerically tractable. Nevertheless, for small aggregates, say $N=5$ with n_e as large as 9, we found that we could run calculations with n_g of up to 4. Of course, the values of n_g and n_e necessary for convergence depend strongly on the Huang–Rhys factor; here we used $X\leq 1$. In test calculations, we found that with $n_g=4$ and $n_e=9$, the time-dependent excitation probability, even in the intermediate coupling regime, is well converged within the time range considered. We note that, as said in Ref. 42, the CES approximation is exactly equivalent to performing a basis set expansion with the restriction that $n_g=1$. Hence, calculations presented in this subsection for $n_g=1$ will be denoted as the CES approximation. First we consider a circular aggregate of five monomers ($N=5$), numbered along the aggregate beginning with the initially excited monomer 0. In Fig. 2 left, $P_{n0}(t)$ is plotted for extreme strong coupling of $2V=10$. Actually on each curve three results, for increasing vibronic coupling, $X=0$, 0.3, and 1.0 are plotted but they are undistinguishable for this coupling strength. Note that $X=0$ gives only the zero-zero vertical transition and so gives results identical to the purely electronic case. Then, as one might expect, there is a smooth movement of the excitation peak along the monomer chain as time progresses. The population of monomer 0 is roughly halved after a time T_{el}, falls

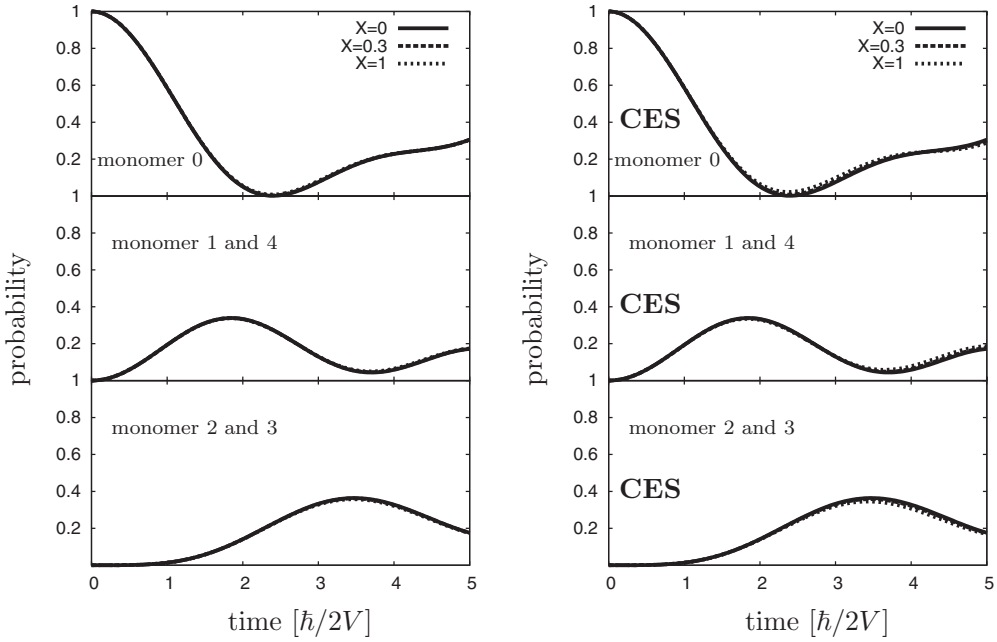

FIG. 2. Excitation probability as a function of time, in units of T_{el} for a ring with $N=5$. Left figure: with $n_g=4$; right figure: CES result ($n_g=1$). Here $2V=10\hbar\omega$ and $n_e=9$. The values for X are indicated in the figures.

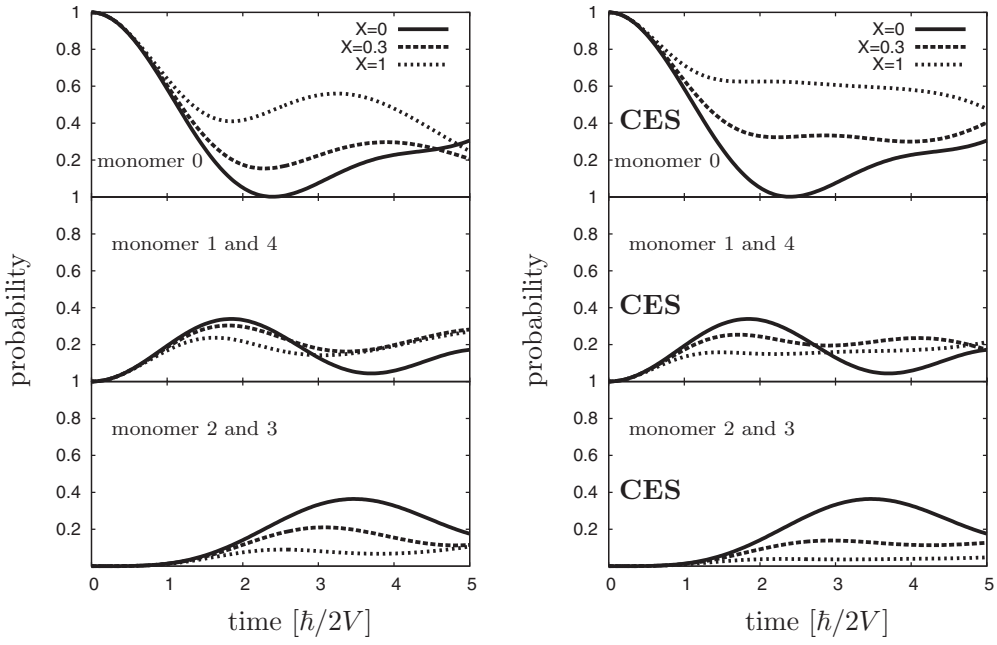

FIG. 3. Same as Fig. 2 but with $2V=1\hbar\omega$.

to zero but then revives at later times. As we shall see, this oscillatory behavior of the excitation probability is typical of strong coupling. On the right set of figures in Fig. 2 the CES results for $n_g=1$ are shown and one notes that in strong coupling, exact and CES approximation are in almost perfect agreement. The intermediate coupling case is where vibronic effects are most pronounced and in Fig. 3 the $P_{n0}(t)$ are shown for the same parameters as in Fig. 2 except that now $2V=1.0$. Since the $X=0$ case is purely electronic, on the scaled time $(2V/\hbar)t$, these curves are identical to those in Fig. 2. Now, however, as X increases, there occurs a pronounced slowing down of excitation transfer so that about 50% probability remains on monomer 0 and only about 10% reaches monomer 3. Although the curves in Fig. 3 (left) are for $n_g=4$, the $n_g=1$ CES results in Fig. 3 (right) are in fair qualitative agreement even for this case of intermediate coupling. Again from Fig. 3 (right), one sees an overall slowing of transfer with increasing X, i.e., with stronger vibronic coupling. The weak electronic coupling case is shown in Fig. 4. Here one sees clearly the damping effect of vibronic coupling on the rate of excitation transfer. In Fig. 4 (bottom), in contrast to the strong-coupling case in Fig. 2 (bottom), one sees that monomer 3 is only maximally $\sim$10% excited for $X=1.0$, whereas in strong coupling, this value is around 30%. The CES results are given in Fig. 4 (right) and again are in excellent agreement with the exact results. For weak cou-

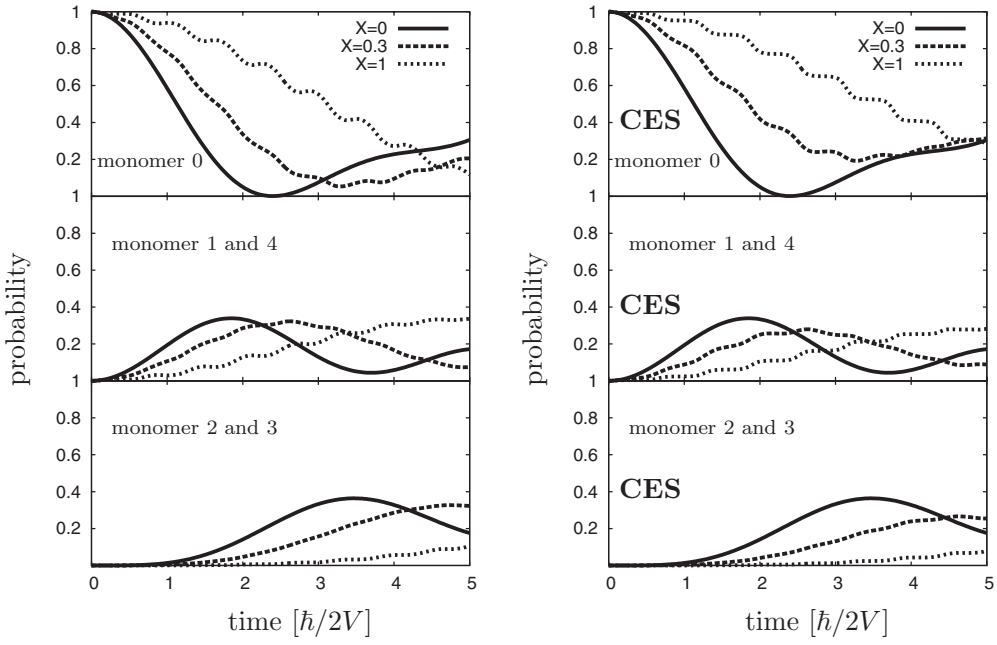

FIG. 4. Same as Fig. 2 but with $2V=0.1\hbar\omega$, i.e., weak electronic coupling.

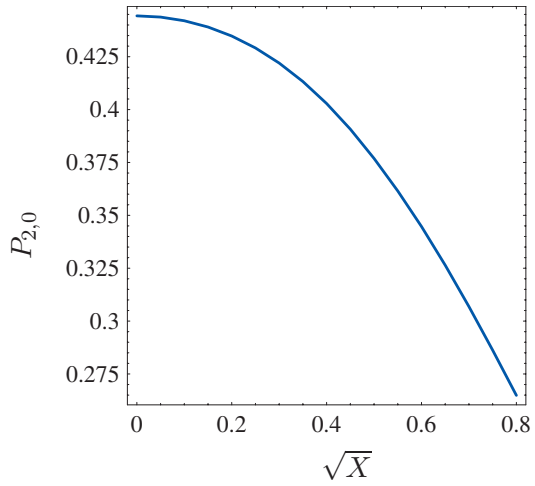

FIG. 5. Magnitude of the first maximum at monomer 2 as a function of $\sqrt{X}$ with $2V=2$ for a linear chain with $N=5$. The calculation has been made with $n_g=2$ and $n_e=5$.

pling, the same agreement was found between absorption spectra calculated by full diagonalization and in CES approximation.[42] A more quantitative picture of the dependence of excitation transfer on X is given in Fig. 5. Here we use the magnitude of the maximum of the first wave front, i.e., the first maximum of the time-dependent excitation probability, at a particular monomer as a measure of the efficiency of excitation propagation. In Fig. 5 the value of the first maximum to reach monomer 2 (when initially starting at monomer 0) is plotted as a function of $\sqrt{X}$ for fixed $2V=2$. Again one sees a strong drop in this probability of excitation as the vibronic coupling parameter increases.

IV. TIME PROPAGATOR IN THE CES APPROXIMATION

A. A single IM vibration: Analytical results

Now we discuss the excitation transfer process solely in the CES approximation since this allows the derivation of simple analytic forms for the excitation propagation probability $P_{n0}(t)$ both in the case of strong and of weak couplings. Furthermore, we can perform numerical calculations for very long aggregates. In discussing excitation transfer analytically, it is also convenient to introduce delocalized exciton electronic states defined as

$$|k\rangle = \frac{1}{\sqrt{N}}\sum_n e^{ikn}|\pi_n\rangle, \tag{19}$$

where $k=2\pi(j-1)/N$ and j runs from 1 to N and we have assumed cyclic boundary conditions. Although not necessary, the condition of replacing the linear chain by a circular aggregate will be made in this section since the analytical expressions obtained are simpler than for a finite linear chain, where end effects lead to more complicated formulas.

In order to calculate $G_{n0}(t)|\Sigma_g\rangle$ in Eq. (10), we consider first the Fourier transform to energy space, i.e., the state $G_{n0}(E)|\Sigma_g\rangle$, where $G_{n0}(E)$ satisfies Eq. (15). We assign the initial monomer arbitrarily the number $m=0$ as fixed value. Then we transform from the localized monomer number n to the exciton number k, i.e.,

$$G_{n0}(E) = \langle\pi_n|G(E)|\pi_0\rangle = \frac{1}{\sqrt{N}}\sum_k e^{ikn}\langle k|G(E)|\pi_0\rangle. \tag{20}$$

The interaction matrix element in Eq. (15) is transformed

$$V_{nn'} = \frac{1}{N}\sum_{kk'} e^{ikn-ik'n'}V_{kk'}. \tag{21}$$

If we consider all monomers identical, then, for a ring or linear chain of monomers, it is easily seen that $V_{kk'}$ is diagonal, i.e.,

$$V_{nn'} = \frac{1}{N}\sum_k e^{ik(n-n')}V_k. \tag{22}$$

Substituting Eqs. (22) and (20) into Eq. (15) leads to

$$\langle k|G(E)|\pi_0\rangle = g_0/\sqrt{N} + \langle g\rangle V_k\langle k|G(E)|\pi_0\rangle. \tag{23}$$

To obtain Eq. (23), we have made the CES approximation in which g_n is approximated by its ground-state average and we have used that all monomers are identical, i.e.,

$$g_n \to \langle\Sigma_g|g_n|\Sigma_g\rangle \equiv \langle g_n\rangle \equiv \langle g\rangle. \tag{24}$$

Then, from Eq. (23) one finds $\langle k|G(E)|\pi_0\rangle = N^{-1/2}g_0(1-\langle g\rangle V_k)^{-1}$ so that the operator $G_{n0}(E)$ can be written as

$$G_{n0}(E) = \frac{1}{N}\sum_k e^{ikn}\frac{g_0}{1-\langle g_0\rangle V_k}. \tag{25}$$

Within the spirit of the CES, the operator g_0 also will be represented in the basis of vibrational states of the aggregate with one monomer electronically excited and all others in the ground electronic and vibrational states, i.e.,

$$|\alpha\rangle \equiv |\alpha,0,\ldots,0\rangle = |\chi_0^\alpha\rangle\prod_{n\neq 0}|\xi_n^0\rangle, \tag{26}$$

where $|\chi_0^\alpha\rangle$ is the αth excited vibrational state in the upper monomer potential curve. Then we have

$$g_0(E) = \frac{1}{E-H_{\mathrm{mon}}+i\delta} = \sum_\alpha \frac{|\alpha,0,\ldots,0\rangle\langle\alpha,0,\ldots,0|}{E-E_\alpha+i\delta}, \tag{27}$$

where $E_\alpha-\epsilon_{\mathrm{el}}$ is the energy of the vibrational state α in the upper potential curve and ϵ_{el} is the monomer electronic excitation energy. Performing the average (24), one has

$$\langle g\rangle = \sum_\alpha \frac{|f_0^\alpha|^2}{E-E_\alpha+i\delta}, \tag{28}$$

where $f_0^\alpha=\langle\chi^\alpha|\xi^0\rangle$ is the FC overlap between the initial and the final monomer vibrational states. Substituting Eqs. (27) and (28) into Eq. (25) gives a closed form expression for G_{n0}, i.e.,

$$G_{n0}(E) = \frac{1}{N}\sum_k e^{ikn} \sum_\alpha \frac{|\alpha,0,\ldots,0\rangle\langle\alpha,0,\ldots,0|}{E - E_\alpha + i\delta - V_k \sum_\beta |f_0^\beta|^2 \frac{E - E_\alpha + i\delta}{E - E_\beta + i\delta}}. \tag{29}$$

This closed form result (29) can be evaluated easily in two limits. First, in strong coupling where $2V$ is much larger than the width of the monomer vibrational band, represented by the width of the FC distribution $|f_0^\beta|^2$, we can replace E_β by its average value $\bar{\epsilon}$. Furthermore, since when the probability (10) is formed, the sum over α is also limited to the spread of the monomer vibrational band, we can also replace E_α by the same average value. This corresponds to assuming that the vibrational states which carry oscillator strength are so closely spaced in energy compared to the exciton bandwidth that they can be replaced effectively by a single level at the mean energy $\bar{\epsilon}$. Then, since

$$\sum_\beta |f_0^\beta|^2 = 1, \tag{30}$$

we have

$$G_{n0} \approx \frac{1}{N}\sum_k e^{ikn} \frac{\mathbb{1}_u}{E - \bar{\epsilon} - V_k + i\delta}, \tag{31}$$

where $\mathbb{1}_u$ is the unit operator in the space of upper vibrational states of monomer 0. Our strong-coupling criterion is exactly that of Simpson and Peterson[38] and apart from the unit operator the result (31) is exactly that obtained by ignoring vibrations altogether.

From Eq. (31), one obtains

$$G_{n0}(t) = \mathbb{1}_u \frac{1}{N}\sum_k e^{ikn} \exp\left(-\frac{i}{\hbar}(\bar{\epsilon} + V_k)t\right) \tag{32}$$

and from Eq. (10) the transfer probability

$$P_{n0}(t) = \left|\frac{1}{N}\sum_k e^{ikn} \exp\left(-\frac{i}{\hbar}(\bar{\epsilon} + V_k)t\right)\right|^2, \tag{33}$$

where again we used Eq. (30).

In nearest-neighbor coupling V_k has the simple form $V_k = 2V\cos k$. Then, dropping the unit operator from Eq. (32) since it disappears in the probability (33), we have the purely electronic result

$$G_{n0}(t) = \frac{1}{N}\sum_j \exp\left[i\frac{2\pi}{N}jn - \frac{i}{\hbar}\left(\bar{\epsilon} + 2V\cos\left(\frac{2\pi}{N}j\right)\right)t\right]. \tag{34}$$

Using the generating function for Bessel functions

$$e^{-iz\cos\varphi} = \sum_{l=-\infty}^{\infty} (-i)^l J_l(z) e^{il\varphi}, \tag{35}$$

one obtains

$$G_{n0}(t) = \frac{1}{N} e^{-i\bar{\epsilon}t/\hbar} \sum_{l=-\infty}^{\infty} (-i)^l J_l\left(\frac{2V}{\hbar}t\right) \sum_j e^{i(2\pi/N)j(n-l)}. \tag{36}$$

The monomers on the circular aggregate are enumerated

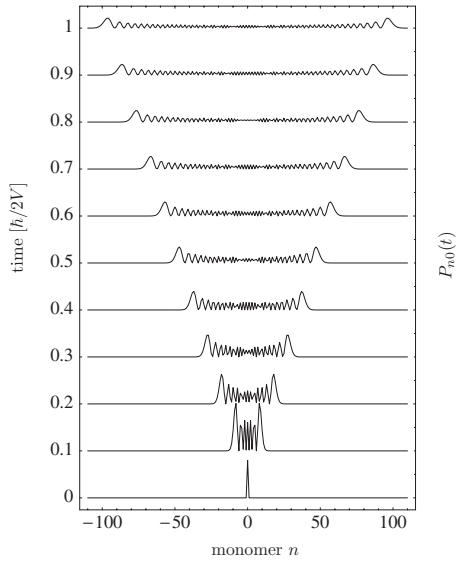

FIG. 6. The probability $P_{n0}(t)$ for strong coupling as a function of n at the times indicated. For better visibility, $P_{n0}(t=0)$ has been reduced to 8% of its real value.

$$N \text{ odd:} \quad -\frac{N-1}{2} \le n \le \frac{N-1}{2},$$
$$N \text{ even:} \quad -\frac{N}{2} + 1 \le n \le \frac{N}{2} \quad \text{or} \quad -\frac{N}{2} \le n \le \frac{N}{2} - 1. \tag{37}$$

To evaluate Eq. (33) further, we consider the limit $N \to \infty$ to obtain the simple result

$$P_{n0}(t) = J_n^2\left(\frac{2V}{\hbar}t\right). \tag{38}$$

This is the result of Merrifield[39] for purely electronic excitation transfer on an infinite linear aggregate. Hence we have shown that, with vibrations, the strong-coupling limit gives the purely electronic result, as one might expect. Note that the time defined by $T_{el} = (\hbar/2V)$ emerges as the natural scale unit for time and corresponds to the electronic excitation transfer time between adjacent monomers when vibrations are not coupled. In Fig. 6, $P_{n0}(t)$, according to Eq. (38), is plotted for a succession of times as a function of monomer number. Then one sees that the leading maximum of the distribution moves roughly linearly with time.

The probability $P_{n0}(t)$ is plotted in Fig. 7 for the case

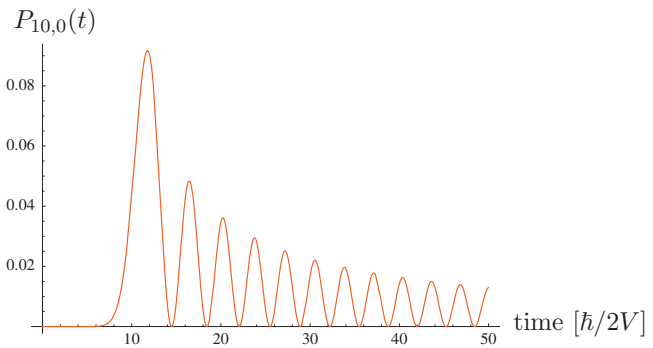

FIG. 7. The probability $P_{10,0}(t)$. The time is in units of $(\hbar/2V)$.

$n=10$ and one sees clearly the oscillatory nature of excitation and de-excitation of a given monomer. This explains the oscillations seen in the numerical results in Fig. 2. One also notes that, due to a simple property of the Bessel functions, the first excitation peak reaches the monomer n at a time which is close to n units of the fundamental time T_{el}, as can be seen in Fig. 7 for the case $n=10$. This property is discussed more fully in Sec. IV B. The mean square displacement is given by the average

$$\overline{n^2(t)} = \sum_{n=0}^{\infty} n^2 P_{n0}(t) = \frac{V^2}{\hbar^2} t^2. \tag{39}$$

If we define $\tilde{n} \equiv \sqrt{\overline{n^2(t)}}$ and the mean propagation velocity $d\tilde{n}/dt$, we see that exciton propagation is at constant velocity $d\tilde{n}/dt=(V/\hbar)$ away from the initial site $n=0$ of excitation.

The second simple analytic limit of Eq. (29) is provided by the case in which the electronic coupling $2V$ is so small that mixing of the vibronic levels in the upper electronic state can be ignored in the propagator. Then only the diagonal term $\beta=\alpha$ in the denominator of Eq. (29) is considered to give

$$G_{n0} \approx \frac{1}{N} \sum_k e^{ikn} \sum_\alpha \frac{|\alpha,0,\ldots,0\rangle\langle\alpha,0,\ldots,0|}{E - E_\alpha - V_k |f_0^\alpha|^2 + i\delta}. \tag{40}$$

Thus, following the steps leading from Eq. (31) to Eq. (38), one has

$$G_{n0}(t) = \sum_\alpha |\alpha\rangle\langle\alpha| e^{-iE_\alpha t/\hbar} (-i)^n J_n\left(\frac{2V}{\hbar}|f_0^\alpha|^2 t\right) \tag{41}$$

and

$$P_{n0}(t) = \sum_\alpha |f_0^\alpha|^2 J_n^2\left(\frac{2V}{\hbar}|f_0^\alpha|^2 t\right). \tag{42}$$

This result was obtained by Bierman[40] using a somewhat more complicated approach than the Green's function method adopted here. Again, one has an oscillatory behavior of the excitation probability with time, in agreement with the weak-coupling numerical results shown in Fig. 4. The result of Eq. (42) can be interpreted simply. In this extreme weak-coupling limit each monomer vibronic level splits into its own exciton band of N levels on aggregate formation but the individual vibronic exciton bands do not overlap. Then excitation transfer occurs resonantly between individual vibronic levels so that the fundamental transfer time is reduced by the factor $|f_0^\alpha|^2$ compared to Eq. (38). Correspondingly, the exciton bandwidth for excited vibrational state α is $2V|f_0^\alpha|^2$, as can be inferred from Eq. (40). From Eq. (42), the average monomer $\sqrt{\overline{n^2(t)}}$ reached at time t is given by the equation

$$\overline{n^2(t)} = \frac{V^2}{\hbar^2} t^2 \sum_\alpha |f_0^\alpha|^6. \tag{43}$$

This result can also be understood in a simple way. Since each vibronic level is independent, from Eq. (39) one would have, for level α

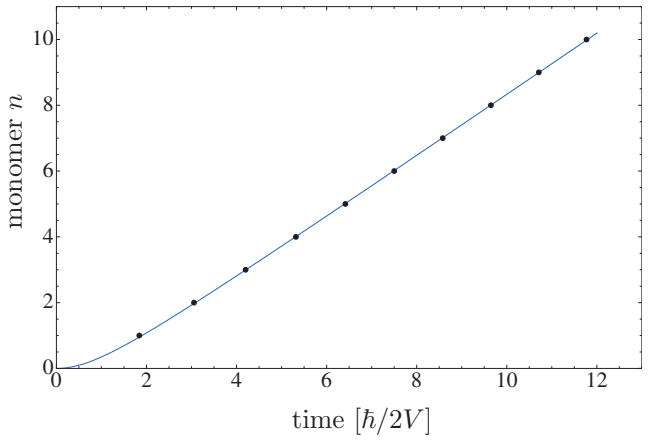

FIG. 8. Time of arrival of the first wave front maximum at monomer n. For $X=0$, i.e., strong coupling.

$$\overline{n_\alpha^2(t)} = \frac{V^2 |f_0^\alpha|^4}{\hbar^2} t^2. \tag{44}$$

Then summing over all levels one has

$$\overline{n^2(t)} = \sum_\alpha \overline{n_\alpha^2(t)} p_\alpha, \tag{45}$$

where p_α is the probability of excitation of level α. However p_α is just given by $|f_0^\alpha|^2$ so from Eqs. (44) and (45) one directly finds the result Eq. (43).

From Eq. (43) one has that the constant mean propagation velocity in this case is $d\tilde{n}/dt=(V/\hbar)(\Sigma_\alpha |f_0^\alpha|^6)^{1/2}$. Since it is readily seen that $\Sigma_\alpha |f_0^\alpha|^6 < 1$, one has the result that even though excitation transfer is at constant velocity, the presence of vibrations leads a lower velocity of propagation then when they are ignored. We note that the simple SP definition of weak coupling is not really appropriate here. In the limit corresponding to the result Eq. (42), one has rather that the vibrational level spacing must be greater than the maximum value of the vibronic exciton bandwidth $2V|f_0^\alpha|^2$. This is an additional condition to the SP criterion.

B. A single IM vibration: Numerical results

Since for the chosen basis the dimension of a full numerical propagation contains the factor n_g^{N-1}, it is not possible to perform full calculations on large aggregates. Happily, however, we have seen that the CES approximation, with $n_g=1$, gives excellent results for weak and strong coupling and qualitatively good results for intermediate coupling. Then we can use formula (29) for $G_{n0}(E)$ to construct numerically $G_{n0}(t)$ and hence calculate $P_{n0}(t)$. Formula (29) depends implicitly on N through the summation over exciton index k. Actually, since the use of formula (29) gives the same results as the numerical procedure with restriction to $n_g=1$, it is simpler to adopt the latter method of calculation.

First let us consider the velocity of the wave front. We return to the purely electronic result Eq. (38) for an infinite chain of monomers. As one sees from Fig. 7, $P_{n0}(t)$ is oscillatory and the time at which a maximum is reached is given by $dP_{n0}(t)/dt=0$. The time of arrival of the first wave front maximum at monomer n is plotted in Fig. 8. The speed is

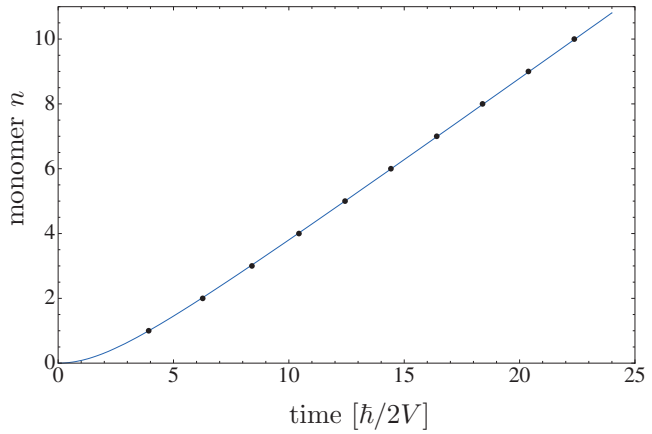

FIG. 9. Time of arrival of the first wave front maximum at monomer n. For weak coupling ($V=0.1$) and $X=0.64$.

rapidly a constant, the wave traveling over ten monomers in around ten time units, i.e., the speed is $2V/\hbar$, which is just twice the mean velocity $d\tilde{n}/dt$. Again we emphasize that the purely electronic result in Fig. 8 is obtained in the vibronic case for $X=0$ and corresponds to the extreme strong-coupling limit.

The case of weak coupling and $N\rightarrow\infty$ gives the analytic result of Eq. (42). Here, a linear relation between n and t is also predicted, as confirmed by the plot in Fig. 9. However, what is noteworthy is the large decrease in the velocity of the wavepacket caused by the presence of FC factors in Eq. (42). In Fig. 9, one sees that a displacement over ten monomers now requires about 25 time units compared to 10 in the pure electronic case in Fig. 8.

Within the weak-coupling limit, it is useful also to examine the X dependence of the $v=n/t$ constant velocity result. One can show that the dependence follows the analytic form $v=n/t=(2V/\hbar)e^{-X}$, indicating a strong reduction in velocity as the vibronic coupling increases. This is in qualitative agreement with Eq. (43) when the rms value $\tilde{n}/t$ is evaluated for the case of a Poissonian distribution of FC factors.

Finally, there is the intermediate coupling case. The $n(t)$ curve for this case is shown in Fig. 10 for $2V=2$ and $X=0.64$. Here a new feature arises in that there are apparent discontinuities in the propagation. A closer inspection of the individual $P_{n0}(t)$ curves (Fig. 11) shows that this is due to the strong vibronic coupling, namely, that the original leading wave front dies out in time and is replaced by the second as "leading" maximum. This smearing of the dominant first maximum is a general feature of vibronic coupling. It occurs around $t=11$ in Fig. 11 and gives rise to an apparent delay in arrival of the wave front. By comparison with the strong-coupling case in Fig. 6, one sees also that when vibronic coupling is present, the wavepacket is spread more evenly among the monomers, indicating that vibrational states of the electronically excited monomer take longer to transfer their energy.

C. Coupling to a vibrational continuum: Numerical results

The final and most important step is to include coupling to the continuous distribution of EM and thereby achieve a more realistic description of the coupling of the electronic excitation to the vibrations of the surroundings, while still retaining the effect of the primary coupling to the IM vibrations. In the standard approach [see point (1) in Sec. I] vibrations are ignored explicitly and calculations are performed for a particular choice of monomer electronic

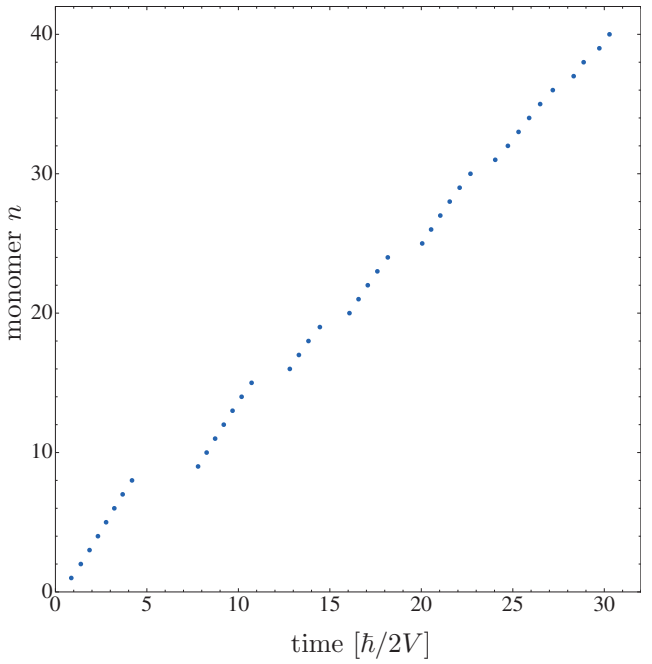

FIG. 10. Time of arrival of the first wave front maximum at monomer n. With $X=0.64$ and intermediate coupling.

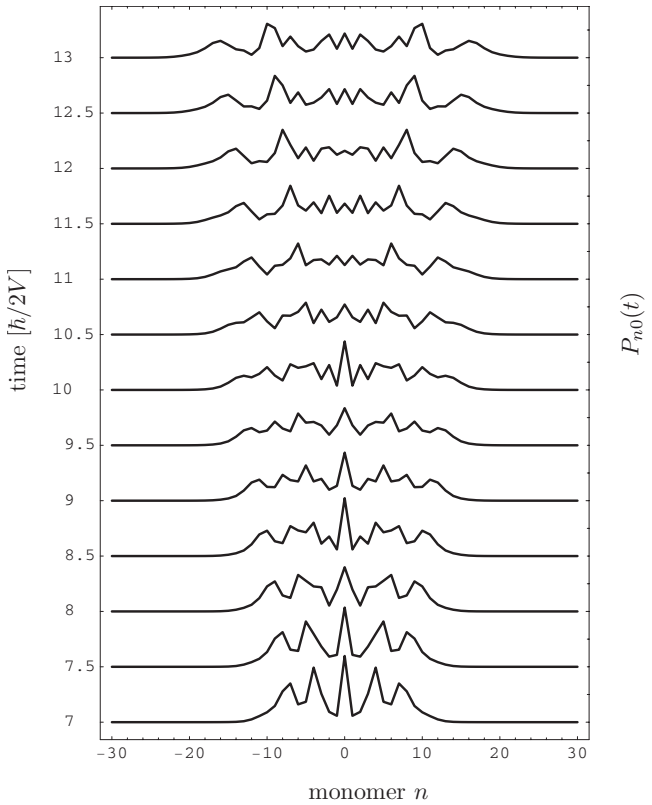

FIG. 11. The distribution $P_{n0}(t)$ as a function of monomer position n shown at successive times.

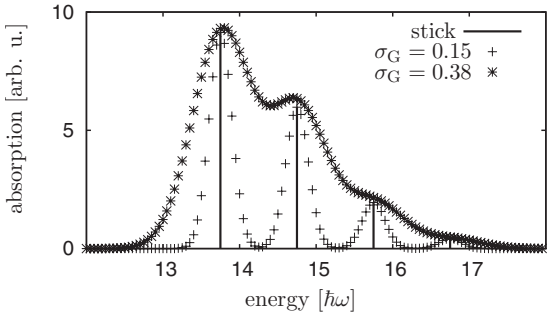

FIG. 12. Poissonian with $X=0.61$ used to fit the measured monomer absorption spectrum of the PIC dye of Ref. 43. Vertical lines, stick spectrum; crosses, convoluted with a Gaussian of width $\sigma_G=0.15$; and stars, with $\sigma_G=0.38$. The energy axis and the values for σ_G are given in units of the stick spacing $\hbar\omega$.

transition energies and/or electronic intermonomer coupling strengths. Then, in the final step, an average is performed over different realizations of this disorder. In this step, the statistical distribution of transition energy (diagonal disorder) and coupling strength (nondiagonal disorder) are taken as fit parameters. Here we seek to make contact with experiment by using the measured monomer continuous spectrum as input. Specifically, we include a primary IM vibration but then we clothe each vibronic level of the monomer with a sequence of densely packed discrete EM transitions, giving rise to an effective continuum of vibronic transitions. As with statistical disorder, this procedure leads to a continuum of possible transition energies along the chain and, through the continuous variation of FC factors, to a continuous distribution of coupling strength between adjacent monomers. Again, as with statistical disorder, the character of this assumed continuous distribution is arbitrary. However, here we choose the distribution specifically to reproduce the experimental isolated-monomer continuous absorption spectrum. An example is shown in Fig. 12, where we fit the measured continuous spectrum of the PIC monomer.[43] The experimental data suggest a single (effective) primary IM mode shown by the fitted discrete "stick" spectrum. In the next step, each of the four vibronic peaks is folded with a Gaussian continuous distribution of width σ_G. Shown in Fig. 12 are the cases $\sigma_G=0.15$ and $\sigma_G=0.38$ (in units of the stick spacing $\hbar\omega$). This latter value gives an excellent reproduction of the experimental spectrum (not shown).[43,44] Since the vibrational basis only manifests itself in the Hamiltonian equation (17) through the monomer vibrational energies and the corresponding FC factors and since the monomer absorption spectrum provides these factors, the remaining step is simply to take the FC distribution in Fig. 12 as a quasicontinuous distribution. The $P_{n0}(t)$ calculated using the continuous distributions of FC factors is shown in Fig. 13. Here we took 120 discrete values to represent the continuous distribution in Fig. 12. The aggregate in this case is a linear chain of 50 monomers with monomer 0 placed at one end and only propagation over one-half of the aggregate displayed for times for which the other end has not been reached. The values of $2V$ and the width σ_G of the individual Gauss peaks is indicated on the figures. In color-coded form, the figures show the electronic excitation probability of a given monomer as a function of time. The figures in the first row [Figs. 13(a)–13(c)], show an extreme strong-coupling case. The pattern is that of Fig. 6 and is the analytic Bessel function result for pure electronic excitation given by Eq. (38). Also shown on the figure as a continuous line is the displacement $\tilde{n}(t)=\sqrt{n^2(t)}$ demonstrating the linear behavior expected. This regular oscillatory pattern is identical in Figs. 13(a)–13(c), showing that the extreme strong-coupling, purely electronic result has been achieved. However, already for $2V=10$, corresponding to a SP parameter of SP$\approx$12, one sees deviations from the Merrifield result, as shown in Figs. 13(d)–13(f). Although the pattern is still regular, at larger times the second maximum becomes more pronounced than the first and there is a slowing of the velocity of propagation, indicated by the decreasing slope of the $\tilde{n}$ line, which becomes more pronounced as the continuous width σ_G increases. This trend is emphasized as the coupling becomes somewhat weaker [Figs. 13(g)–13(i)] with $2V=5$ corresponding to SP$\approx$6. In the course of time, the probability becomes more smeared out over the whole aggregate, although regularity is still discernible. Note that the width of the monomer absorption spectrum is mainly determined by the width stemming from the primary vibrational mode with $X=0.61$. The convolution with the continuous Gaussian changes the overall width only slightly. For example, in the case $2V=5$ one has a SP parameter SP=6.4 for the stick spectrum and SP=5.7 for the spectrum with $\sigma_G=0.38$.

The cases in Figs. 13(j)–13(l) approach an intermediate coupling, with SP$\approx$3. One sees, for the stick spectrum in Fig. 13(j), a general smearing out of an irregular probability pattern and a pronounced concentration of probability remaining around the origin. This tendency increases dramatically as the continuous width is increased [Figs. 13(k) and 13(l)]. Although the propagation velocity $(\tilde{n}/t)$ reduces considerably with the width, it still remains finite, indicating that there is still a continuing transfer of probability along the chain. However, comparison of Figs. 13(j)–13(l) shows for the first time the new effect arising from transition to a continuous spectrum or, equivalently, strong coupling to external modes. There is a marked tendency, not evident in the case of a stick monomer spectrum, for excitation to remain trapped on the first few monomers.

The trapping of excitation becomes increasingly pronounced when $2V$ is reduced to give intermediate and weak coupling, and the width σ_G is increased. This is shown in Figs. 13(m)–13(r). For $2V=1$, the stick spectrum gives irregular propagation but for $\sigma_G=0.38$ [Fig. 13(o)], there is a complete collapse of propagation and $\tilde{n}$ becomes constant in time. Finally, for the case of weak coupling the transition to a continuous spectrum becomes even more dramatic. Figures 13(p)–13(r) are for the case SP=0.6. For the stick spectrum [Fig. 13(p)], constant velocity propagation is recovered and the pattern of probability change is becoming regular, corresponding to a slow approach to the Bierman, case of Eq. (42). By contrast, even for $\sigma_G=0.15$, when the spectrum of the monomer is continuous, excitation remains trapped near the origin and increasingly so as the continuous width increases.

One can question the physical origin of the trapping

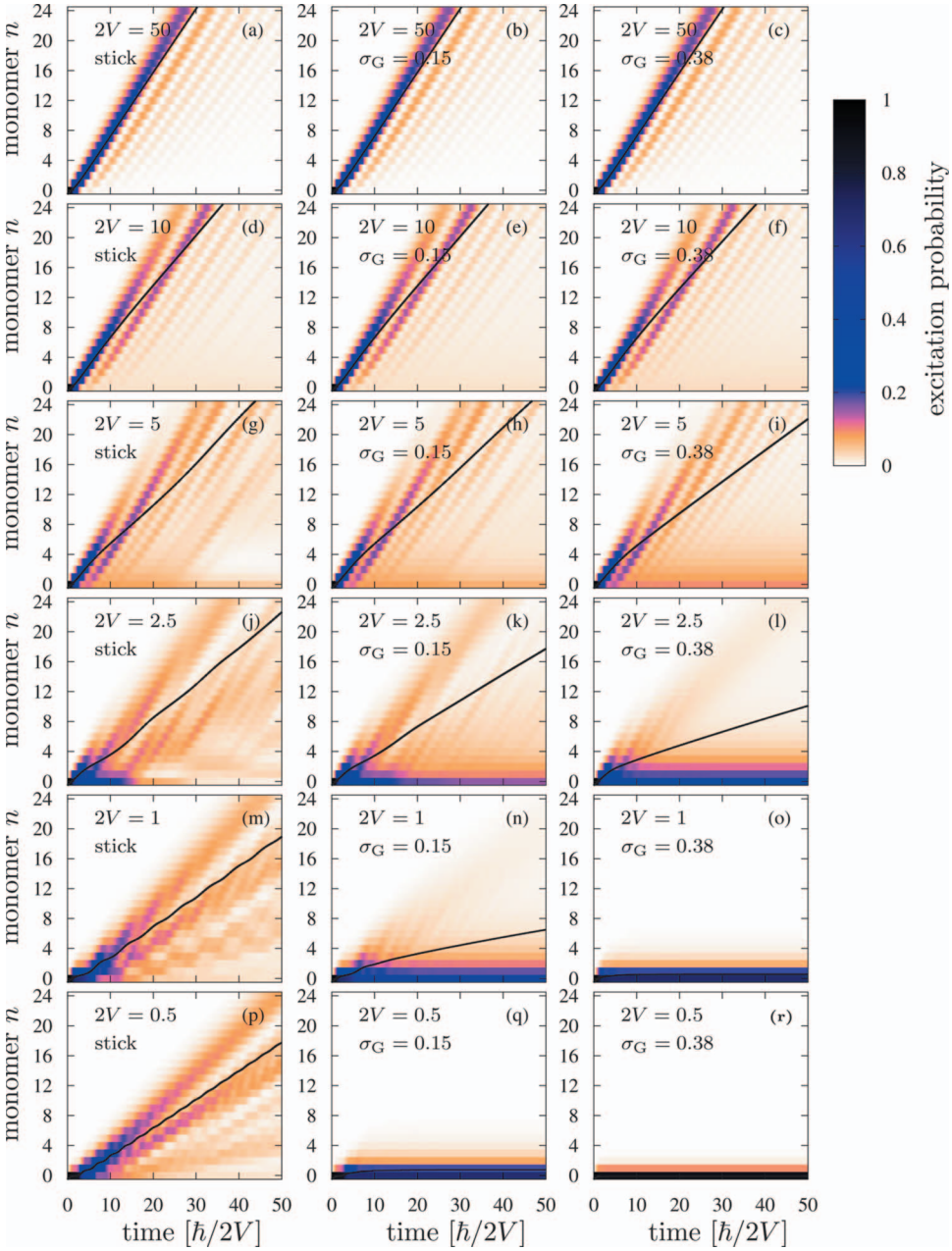

FIG. 13. Probability $P_{n0}(t)$ that monomer n is electronically excited at time t. The aggregate is a linear chain of $N=50$ monomers (only one-half of the aggregate is shown here). The values for $2V$ and the convolution width σ_G of the monomer spectrum are indicated on the figures. The continuous line shows $\tilde{n}(t)$.

mechanism. As we show explicitly in Sec. IV D, this is readily understood. A discrete set of oscillator eigenstates in the upper potential, giving rise to a stick spectrum, requires the establishment of repeated oscillation, in principle, for an infinite time, in the upper potential well. Clearly, any coupling to other modes leads to a broadening of the absorption line. Coupling to very many densely packed EM leads to an effective continuum broadening. In the time picture, this can be mimicked by considering that a time-dependent vibrational wavepacket is formed in the upper state. If the wavepacket reflects back and forth many times in a potential well, vibrational eigenstates are formed and the absorption spectrum is structured. A structureless absorption continuum would then correspond to the extreme situation that the wavepacket moves out of the region of overlap with vibrational states of the ground electronic state and does not return [see Fig. 1(b)]. In this way the coupling to EM is represented by an effective repulsive BO potential in the upper state. The electronic excitation can only be transferred during the time when there is overlap between ground-state and excited-state vibrational wavepackets. For longer times the FC factor is zero and the excitation remains trapped. In the following we derive a simple analytic model which explains the trapping phenomenon.

D. Coupling to a vibrational continuum: The Magee–Funabashi approximation

We have seen from the numerical results of Sec. IV C that the transition to a continuous spectrum has a profound effect on the character of exciton propagation. In particular, for intermediate coupling, we observe a trapping of the exciton at a time characteristic of the electronic coupling strength and the width of the vibronic spectrum, which itself is a measure of the strength of the intramonomer vibronic coupling. Now we will show how an approximate analytic

result can be derived in CES approximation, which allows a simple physical interpretation of the trapping predicted by the numerical results of Sec. IV C to be given. In Appendix A it is shown that the probability that electronic excitation has reached monomer n is given by,

$$P_{n0}(t) = |J_n(\gamma(t))|^2, \tag{46}$$

where

$$\gamma(t) = (2V/\hbar)\int_0^t F(t')dt'. \tag{47}$$

One notes that the argument $\gamma(t)$ of the Bessel function now appears as $1/T_{\rm el}$ multiplied by the time integral of $F(t)$, which, as defined in Appendix A, is just the time-dependent FC factor $F(t)$ reflecting the overlap between vibrational wave functions in ground and excited electronic states. Although this result is analytic and appealingly simple and although not readily seen from the derivation given by Magee and Funabashi,[41] the final approximation leading to Eq. (A8) of Appendix A is somewhat drastic in that it demands that, for fixed time, the FC factors between monomer n and both neighbors $n\pm 1$ are identical.

We consider three special cases. The first two provide just the known analytic solutions from Sec. IV A. First we assume the CES approximation that the excited electronic state vibrational wave function is of the form,

$$|\Sigma_e^n(t)\rangle = |\chi_n(t)\rangle \prod_{m\neq n} |\xi_m^0\rangle \tag{48}$$

and, see Appendix A,

$$F(t) = \langle \Sigma_e^n(t)|\Sigma_e^{n\mp 1}(t)\rangle = \langle \chi_n(t)|\xi_n^0\rangle\langle \xi_{n\pm 1}^0|\chi_{n\pm 1}(t)\rangle. \tag{49}$$

The wavepacket $|\chi_m(t)\rangle$ is that produced upon vertical electronic excitation of monomer m from the ground vibrational state $|\xi_m^0\rangle$. The initial condition is $|\chi_n(0)\rangle = |\xi_n^0\rangle$ and then the wavepacket develops in time in the excited-state potential curve. In the first case, the extreme strong-coupling limit, the excitation is passed on to the neighboring monomer before there is any time for the wavepacket to change. Then $F(t)=1$ and $\gamma(t)=(2V/\hbar)t$, exactly the result of Eq. (38). In the second case we consider only a single vibrational eigenstate α in the upper potential curve. Then $F(t)=|f_0^\alpha|^2$ and the probability for coherent excitation transfer is

$$P_{n0}^\alpha(t) = J_n^2\left(\frac{2V}{\hbar}|f_0^\alpha|^2 t\right). \tag{50}$$

The total probability, starting from an initial distribution $p_\alpha = |f_0^\alpha|^2$ is given by

$$P_{n0}(t) = \sum_\alpha |f_0^\alpha|^2 J_n^2\left(\frac{2V}{\hbar}|f_0^\alpha|^2 t\right), \tag{51}$$

which is identical to Bierman's result of Eq. (42), the extremely weak-coupling case.

The third and most important case is where we consider a continuous monomer absorption spectrum, corresponding to coupling to EM vibrations. It is clear that the absence of discrete vibrational structure indicates that the wavepacket $\chi(t)$ does not oscillate back and forth in the upper BO potential curve, as is necessary for the formation of eigenstates. Rather the continuum in energy space corresponds to a wavepacket which moves out continually in space and does not return. This behavior mimics the continuous broadening of the vibrational eigenstates due to coupling to the continuous spectrum of EM vibrations. The simplest way to model this behavior is to take, not a harmonic potential but a simple linear potential in the upper state [see Fig. 1(b)]. The monomer absorption spectrum is proportional to $-\mathrm{Im}\langle g(E)\rangle$. For example, from Eq. (28), we have

$$\mathrm{Im}\langle g(E)\rangle = \pi\sum_\alpha |f_0^\alpha|^2 \delta(E-E_\alpha), \tag{52}$$

showing absorption in discrete spectral lines. By contrast, in the continuous case for a linear potential, from Eq. (B6) of Appendix B one has, in terms of the dimensionless energy ϵ (defined in Appendix B),

$$\mathrm{Im}\langle g(\epsilon)\rangle \propto e^{-\epsilon^2}, \tag{53}$$

which is a continuous single Gaussian absorption spectrum. Clearly, more complicated vibronic absorption spectra can be fitted by a sum of such Gaussians. From Eqs. (48) and (49), one sees that, taken independent of n, the function $F(t)$ is given by

$$F(t) = |\langle \chi(t)|\xi^0\rangle|^2 = |\langle \xi^0|g(t)|\xi^0\rangle|^2 \equiv |\langle g(t)\rangle|^2 \tag{54}$$

so that, from Eq. (47) and Eq. (B7) of Appendix B, we have

$$\gamma(t) = \frac{2V}{\hbar}\int_0^t \exp\left[-\left(\frac{t'}{T_{\rm vib}}\right)^2\right]dt' = \frac{2V}{\hbar}\frac{\sqrt{\pi}}{2}T_{\rm vib}\ \mathrm{erf}\left[\frac{t}{T_{\rm vib}}\right], \tag{55}$$

where $T_{\rm vib}=\hbar/\sigma_G$ can be thought of as a characteristic vibronic coupling time since σ_G is the width of the Gaussian vibronic absorption spectrum. This general result satisfies two limits. The first is the limit $t\to 0$ when $\mathrm{erf}(t/T_{\rm vib}) \to (2/\sqrt{\pi})(t/T_{\rm vib})$ so that $\gamma=(2V/\hbar)t$ and we recover the strong-coupling case, where the initial wavepacket has no time to move before it is handed on. The second limit is $(t/T_{\rm vib})\to\infty$ when $\mathrm{erf}(t/T_{\rm vib})\to 1$ and we have

$$\gamma(t) = \frac{2V}{\hbar}\frac{\sqrt{\pi}}{2}T_{\rm vib} \approx \frac{T_{\rm vib}}{T_{\rm el}} = \frac{2V}{\sigma_G}. \tag{56}$$

Hence, this theory predicts that at large times a fixed probability distribution $P_n(\gamma)$ emerges, i.e., the exciton becomes trapped. Clearly the realization of this long-time limit for a single monomer requires that the excitation is not transferred to a neighbor within this time, i.e., that $T_{\rm vib}/T_{\rm el}\leq 1$. That is, as the numerical solutions show, only in weak and intermediate coupling, is there trapping of the exciton. Note also that, for a continuous spectrum, the extremely weak-coupling case of Bierman, which requires the condition $2V\leq\hbar\omega$, will not occur since effectively $\omega\to 0$.

To illustrate that the analytic approximation explains the trapping we have calculated $P_{00}(t)=|J_0(\gamma(t))|^2$ using Eq. (49) and Eq. (B8) of Appendix B. The result shown in Fig. 14 is compared with the result of the CES approximation numeri-

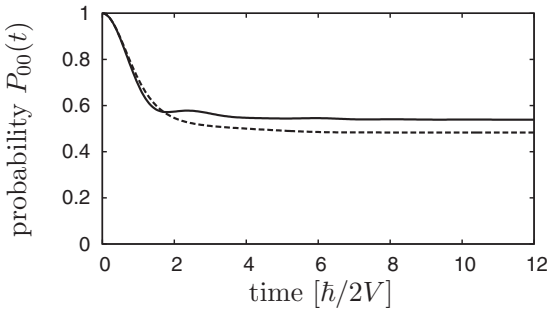

FIG. 14. The probability $P_{00}(t)$ that excitation resides on monomer zero as a function of time in units of T_{el}. The parameters are $2V=1$, $\sigma_G=0.38$, and $X=0.61$ [corresponding to Fig. 13(o) and the broadest spectrum in Fig. 12]. Solid line: CES approximation. Dashed line: Magee–Funabashi approximation.

cal calculation for the case shown in Fig. 13(o). Clearly one sees that the analytic Magee–Funabashi approximation gives a good description of the rate of approach to a time-independent probability, i.e., trapping of the excitation.

Finally we discuss the mean velocity of propagation of the electronic excitation. The mean square propagation distance is given by

$$\overline{n^2(t)} = \sum_{n=0}^{\infty} n^2 |J_n(\gamma(t))|^2 = \gamma^2(t)/4. \tag{57}$$

Hence,

$$\tilde{n}(t) = \gamma(t)/2 = (V/\hbar)\int_0^t |\langle g(t')\rangle|^2 dt' \tag{58}$$

and the time-dependent mean velocity is

$$\frac{d\tilde{n}}{dt} = (V/\hbar)|\langle g(t)\rangle|^2. \tag{59}$$

For a discrete monomer spectrum $\langle g(t)\rangle$ is calculated easily by Fourier transform of $\langle g(E)\rangle$ of Eq. (28) to give

$$\langle g(t)\rangle = \sum_{\alpha} |f_0^{\alpha}|^2 \exp(-iE_{\alpha}t/\hbar). \tag{60}$$

Three points are noteworthy here.

(1) If the distribution with width $\sigma=\sqrt{X}\hbar\omega$ is small with respect to $2V$, we can replace E_{α} by the average energy $\bar{\epsilon}$. This leads to $\langle g(t)\rangle=\exp(-i\bar{\epsilon}t/\hbar)$ and to the strong-coupling pure electronic result $d\tilde{n}/dt=V/\hbar$, as expected.

(2) In general, one has

$$\frac{d\tilde{n}}{dt} = (V/\hbar)\sum_{\alpha}\sum_{\beta} |f_0^{\alpha}|^2 |f_0^{\beta}|^2 \exp[-i(E_{\alpha}-E_{\beta})t/\hbar]. \tag{61}$$

This illustrates that the reduction in velocity encountered when the single electronic transition is split into many vibronic (but still discrete) transitions is due to a dephasing arising from the many different frequencies in the double sum in this equation for the velocity. The number of vibronic levels involved in the sum increases with increasing vibronic coupling (increasing X), which explains the strong reduction of propagation velocity with increasing X shown in Fig. 5

(3) In the continuum limit $X\to\infty$ and $\omega\to 0$ with σ constant, the FC Poissonian distribution of Eq. (1) becomes a Gaussian distribution in energy, corresponding to the linear potential result of Eq. (53). Correspondingly, the Fourier series Eq. (60) becomes the Fourier transform of a continuous Gaussian distribution leading to the time-dependent Gaussian $\langle g(\tau)\rangle=\exp(-\tau^2/2)$ of Eq. (B7), where τ is the dimensionless time $\tau=t/T_{vib}$. This correspondence justifies our numerical procedure of treating the continuum as a very large number of densely packed discrete transitions. One can also interpret the trapping phenomenon arising from a continuous spectrum as due to the interference of infinitely many phase factors appearing in Eq. (61) which damps out the propagation at large τ, i.e., large times $t \gg T_{vib}$.

V. CONCLUSIONS

We have examined the transfer of electronic excitation (EET) on a chain of molecules which interact via electronic coupling and which have a ground and one excited electronic level. The electronic levels are considered to couple both to internal vibrational modes of the monomer (IM) and EMs of the surroundings. The IM are specified as giving a single dominant vibrational progression, as seen, for example, in the monomer spectrum of many dye molecules forming large aggregates. The EMs are not included specifically but are assumed to give rise to a continuous vibronic absorption spectrum, again typical of many organic molecules in solution.

The probability $P_n(t)$ that, beginning with electronic excitation localized on a single monomer, the excitation has propagated a distance of n monomers can be expressed in terms of matrix elements of the time propagator or time-dependent Green's operator $G(t)$. Initially, for small aggregates and a single discrete IM vibration, we have performed the time propagation exactly numerically. For strong coupling (SP$\to\infty$), which corresponds to the limit of vanishing vibronic coupling ($X\to 0$), $P_n(t)$ shows an oscillatory behavior. The effect of increasing vibronic coupling is to damp the amplitude of the oscillations and to lengthen their period. The net result is an effective slowing or inhibition of the migration of the excitation away from the initial site. Nevertheless, in the course of time the excitation propagates over

the complete aggregate. The CES approximation, which restricts the occupation to the lowest vibrational state of the ground electronic state, has been shown to give good overall agreement with the exact results. This approximation has the advantage that extremely long aggregates (of the order of 100 monomers) can be handled numerically and, in certain limits, analytical solutions for matrix elements of $G(t)$ can be obtained. Taking advantage of this simplification and with a combination of numerical and analytical solutions we have established the following characteristics of the propagation of vibronic excitation.

(1) In the pure electronic case, excitation is an oscillatory function of time and propagates with constant mean velocity from the site of initial excitation. This characteristic is largely retained when vibronic coupling is included but $\mathrm{SP} \gg 1$, i.e., strong coupling.
(2) In the case of a discrete spectrum (single IM vibration), for intermediate coupling the regular pattern of propagation is destroyed, probability becomes smeared out in an irregular fashion, and there is a reduction in the mean velocity of propagation.
(3) In the case of a discrete spectrum, for weak coupling, a quasiregular pattern of propagation is restored (in agreement with the analytical result of Bierman) but at a considerably lower velocity than that predicted by the purely electronic case.
(4) The above features can all be explained by approximate analytic solutions in which $P_n(t)$ is expressed in terms of Bessel functions. In particular, the constant velocity limits in strong and weak couplings are explained. The inhibition and irregularity of propagation in the intermediate coupling case is shown to be due to a dephasing arising from the many different pathways of transfer between adjacent monomers when many vibronic levels participate.
(5) When coupling to EM is included by a transition to a continuous spectrum, a new phenomenon appears in the numerical solutions in that, in the course of time, the propagation velocity goes to zero, i.e., the exciton becomes trapped with a fixed distribution P_n independent of time. This trapping has also been explained analytically by a simple model of an upper linear BO potential such that the vibrational wavepacket moves out from the FC overlap region with the ground BO potential and does not return. Then the trapping time is just the time taken for the overlap to go to zero, which turns out to be on the order of $\hbar/\sigma$, where σ is the width of the continuous monomer vibronic spectrum.

Our aim in this study has been not to give a detailed numerical simulation of any particular EET process but to establish the main characteristics of EET coupled to vibrations and to isolate the physical parameters governing these characteristics. To simplify the study of propagation, we have assumed that electronic excitation is localized initially on a single monomer. However, in a real experiment it is probable that light absorption leads to simultaneous finite probability of many monomers, i.e., an initially delocalized exciton. Hence the rather small transfer distances that are predicted before trapping when the spectrum is broad and continuous may not indicate that excitation is localized over such distances.

It must also be pointed out which physical processes are not taken into account here. In this respect the major omission is that of coupling between the vibrational degrees of freedom, whether IM or EM, themselves. This will lead to dissipation of the energy of excitation and accumulation of probability in the lowest vibrational states of each BO potential. Similarly, finite temperature will alter the occupation of vibronic levels. In the case of the trapping of excitation predicted when the vibronic spectrum is continuous, we have not considered the further fate of the wavepacket after leaving the FC region. Clearly, coupling to other processes, e.g., dissociation of the exciton, presence of acceptor molecules, and radiative decay, will disturb the establishment of a time-independent probability distribution of the electronic excitation. However, the model can be extended, albeit numerically, to include such couplings. Also the CES approximation used ignores part of the vibrational structure of the ground electronic state, which may also play a role in the transfer dynamics. Finally, to expose more clearly the main physical mechanisms operating, we have restricted discussion to the simplest geometry, that of a linear or circular chain of monomers. In applications the precise geometry of the three-dimensional aggregate must be taken into account, usually giving a larger number of nearest or near neighbors between which EET can occur. In some cases, e.g., Refs. 7 and 45, an effective linear geometry appears a good approximation; however, in others, e.g., Refs. 46–49, the aggregate is two or three dimensional.

Since this is a model study, the main results are not restricted to the particular case of an aggregate of electronically coupled large organic molecules. In particular, the analytical approximations should be applicable to other quantum aggregates modeled by two-level monomers with superimposed vibrational structure, such as are listed in Sec. I.

ACKNOWLEDGMENTS

Financial support of this work by the DFG under Project No. Br 728/11 is gratefully acknowledged.

APPENDIX A: DERIVATION OF THE MAGEE-FUNABASHI FORMULA

We differentiate Eq. (3) of the text and obtain (for times $t>0$)

$$\frac{\partial}{\partial t}G(t) = -\frac{i}{\hbar}HG(t). \tag{A1}$$

Taking electronic matrix elements and inserting a unit operator between H and $G(t)$, one gets

$$\frac{\partial G_{nm}(t)}{\partial t} = -(i/\hbar)\sum_{n'} H_{nn'}G_{n'm}(t) = -(i/\hbar)\sum_{n'} V_{nn'}G_{n'm}(t) - (i/\hbar)K^{n}_{\mathrm{mon}}G_{nm}(t), \tag{A2}$$

where K^{n}_{mon} is a sum of single monomer BO vibrational Hamiltonians with monomer n excited electronically (ϵ_{el} is taken as the arbitrary zero of energy). This equation remains an operator equation in the space of vibrational coordinates. To remove the last term in Eq. (A2) we define a time-dependent vibrational state $|\Sigma^{n}_{e}(t)\rangle$ of the polymer by the equation

$$\left(K^{n}_{\mathrm{mon}} - (i/\hbar)\frac{\partial}{\partial t}\right)|\Sigma^{n}_{e}(t)\rangle = 0. \tag{A3}$$

Then, we have

$$\frac{d}{dt}\langle\Sigma^{n}_{e}(t)|G_{nm}(t)|\Sigma_{g}\rangle = \langle\Sigma^{n}_{e}|\frac{\partial G_{nm}(t)}{\partial t}|\Sigma_{g}\rangle + \left\langle\frac{\partial\Sigma^{n}_{e}}{\partial t}|G_{nm}(t)|\Sigma_{g}\right\rangle. \tag{A4}$$

Taking the appropriate matrix element of Eq. (A2), we obtain

$$\frac{d}{dt}\langle\Sigma^{n}_{e}(t)|G_{nm}(t)|\Sigma_{g}\rangle = -(i/\hbar)\sum_{n'} V_{nn'}\langle\Sigma^{n}_{e}(t)|G_{n'm}(t)|\Sigma_{g}\rangle. \tag{A5}$$

Since the coupling matrix element on the right hand side of the above equation involves both n and n' it is not possible to proceed further without approximation. Since the operator $G_{n'm}$ places monomer n' in the excited electronic state, one introduces, as an approximation to the unit operator, the projector $|\Sigma^{n'}_{e}(t)\rangle\langle\Sigma^{n'}_{e}(t)|$ into the coupling term, i.e.,

$$\frac{d}{dt}\langle\Sigma^{n}_{e}(t)|G_{nm}(t)|\Sigma_{g}\rangle = -(i/\hbar)\sum_{n'} V_{nn'}\langle\Sigma^{n}_{e}(t)|\Sigma^{n'}_{e}(t)\rangle\times\langle\Sigma^{n'}_{e}(t)|G_{n'm}(t)|\Sigma_{g}\rangle. \tag{A6}$$

Then, restricting to nearest-neighbor coupling, arbitrarily fixing $m=0$ and taking $V_{n,n-1}=V_{n,n+1}=V$ for identical monomers, one has the set of equations,

$$\frac{d}{dt}b_{n}(t) = -(i/\hbar)V[\langle\Sigma^{n}_{e}(t)|\Sigma^{n-1}_{e}(t)\rangle b_{n-1}(t) + \langle\Sigma^{n}_{e}(t)|\Sigma^{n+1}_{e}(t)\rangle b_{n+1}(t)], \tag{A7}$$

where we have set $b_{m}=\langle\Sigma^{m}_{e}(t)|G_{m0}(t)|\Sigma_{g}\rangle$. The final approximation is to take $\langle\Sigma^{n}_{e}(t)|\Sigma^{n\mp1}_{e}(t)\rangle=F(t)$ to be independent of n. This approximation leads to the simple set of coupled equations,

$$\frac{d}{dt}b_{n}(t) = -(i/\hbar)VF(t)[b_{n-1}(t) + b_{n+1}(t)]. \tag{A8}$$

As Magee and Funabashi[41] showed, these coupled equations have the solution,

$$b_{n}(t) = \exp(-in\pi/2)J_{n}(\gamma(t)), \tag{A9}$$

where

$$\gamma(t) = (2V/\hbar)\int_{0}^{t} F(t')dt'. \tag{A10}$$

APPENDIX B: THE CONTINUOUS MONOMER ABSORPTION SPECTRUM

The monomer energy-dependent Green's function with the upper BO potential approximated by a linear form with slope a [see Fig. 1(b)] is given by the equation

$$\left(\frac{\hbar^2}{2}\frac{\partial^2}{\partial Q^2} + E - \epsilon_{\mathrm{el}} + aQ + \epsilon_{0}\right)g(Q,Q',E) = \delta(Q,Q'). \tag{B1}$$

The ground-state vibrational potential is assumed harmonic, with rest energy $\epsilon_{0}=\hbar\omega/2$ and with ground eigenfunction,

$$\xi_{0} = (b^{1/2}/\pi^{1/4})\exp(-b^2Q^2/2), \tag{B2}$$

where $b^2=2\omega/\hbar$. Transforming to the dimensionless variable $x=bQ$ gives a monomer Green's function defined by

$$\kappa\frac{\partial^2 g}{\partial x^2} + (\epsilon + \kappa + x)g(x,x') = (b^2/a)\delta(x-x'), \tag{B3}$$

where we define the dimensionless quantities $\kappa=\hbar\omega/(2a/b)$ and $\epsilon=(E-\epsilon_{\mathrm{el}})/(a/b)$. In Ref. 50 it is shown that an integral representation of $g(x,x')$ can be derived from which an integral representation of the ground-state expectation value $\langle g(\epsilon)\rangle$ can be calculated, i.e.,

$$\langle g(\epsilon)\rangle = \int_{0}^{\infty}\xi_{0}(x)g(x,x',\epsilon)\xi_{0}(x')dxdx' = -i(a/b)\int_{0}^{\infty}\frac{\exp(-ikx^3/12 - x^2/4)}{(ikx+1)^{1/2}}e^{(i\epsilon x)}dx. \tag{B4}$$

From this form, the Fourier transform to time space is easily performed to give $\langle g(\tau)\rangle$ and

$$|\langle g(\tau)\rangle|^2 = \frac{\exp(-\tau^2)}{(\kappa^2\tau^2+1)^{1/2}}, \tag{B5}$$

where τ is the dimensionless time $\tau=t/T_{\mathrm{vib}}$. Since κ is usually much less than unity, the approximation $\kappa=0$, which amounts to neglecting the kinetic energy near to the turning point, is often a good approximation. Then Eq. (B4) can be evaluated in closed form to give

$$\langle g(\epsilon)\rangle = \frac{b}{a}e^{-\epsilon^2}(2\,\mathrm{erf}(-i\epsilon) - i\sqrt{\pi}), \tag{B6}$$

whose imaginary part gives a continuous Gaussian absorption spectrum (see also Refs. 30 and 31). Correspondingly, for $\kappa=0$, Eq. (B5) reduces to the simple form

$$|\langle g(\tau)\rangle|^2 = \exp(-\tau^2), \tag{B7}$$

showing explicitly that the outgoing motion of the excited-state vibrational wavepacket leads to a decay in time of the effective FC factor for transfer between electronic ground

state and electronic excited state. In the dimensionless time $\tau = t/T_{\text{vib}}$, the scale time T_{vib} is given by $T_{\text{vib}} = \sqrt{2}\hbar/(a/b) = \hbar/\sigma_G$ since $(a/\sqrt{2}b)$ is the width σ_G, in dimensions of energy, of the monomer continuous Gaussian absorption spectrum obtained from Eq. (B6). Hence T_{vib} can be viewed as a typical time for the onset of vibronic coupling.

In the case of Fig. 12 where the absorption spectrum is fitted by a sum of Gaussians, Eq. (B7) must be suitably modified. In this case the spectrum can be viewed as the convolution of a stick spectrum with a set of Gaussians centered at the sticks. Hence, the Fourier transform to time space consists of a product of the separate Fourier transforms of the Gaussian and the stick spectrum. Then it is easy to show that Eq. (B7) is generalized to

$$|\langle g(\tau)\rangle|^2 = \exp(-\tau^2)\left|\sum_{\alpha} |f_0^{\alpha}|^2 \exp(i\epsilon_{\alpha}\tau)\right|^2, \tag{B8}$$

where $\epsilon_{\alpha} = E_{\alpha}/\sigma_G = \alpha(\hbar\omega)/\sigma_G$.

[1] A. Davydov, *Theory of Molecular Excitons* (McGraw-Hill, New York, 1962).
[2] H. Haken and P. Reineker, Z. Phys. **249**, 253 (1971).
[3] H. Haken and G. Strobl, Z. Phys. **262**, 135 (1973).
[4] P. O. J. Scherer, E. W. Knapp, and S. F. Fischer, Chem. Phys. Lett. **106**, 191 (1984).
[5] C. Supritz, V. Gounaris, and P. Reineker, J. Lumin. **128**, 877 (2008).
[6] *J-Aggregates*, edited by T. Kobayashi (World Scientific, Singapore, 1996).
[7] H. van Amerongen, L. Valkunas, and R. van Grondelle, *Photosynthetic Excitons* (World Scientific, Singapore, 2000).
[8] T. Brixner, J. Stenger, H. M. Vaswani, M. Cho, R. E. Blankenship, and G. R. Fleming, Nature (London) **434**, 625 (2005).
[9] O. Kühn and V. Sundström, J. Chem. Phys. **107**, 4154 (1997).
[10] T. Renger and V. May, J. Phys. Chem. A **102**, 4381 (1998).
[11] P. Rebentrost, M. Mohseni, I. Kassal, S. Lloyd, and A. Aspuru-Guzik, New J. Phys. **11**, 033003 (2009).
[12] F. Robicheaux, J. V. Hernández, T. Topçu, and L. D. Noordam, Phys. Rev. A **70**, 042703 (2004).
[13] C. Ates, A. Eisfeld, and J. M. Rost, New J. Phys. **10**, 045030 (2008).
[14] O. Mülken, A. Blumen, T. Amthor, C. Giese, M. Reetz-Lamour, and M. Weidemüller, Phys. Rev. Lett. **99**, 090601 (2007).
[15] G. D. Scholes and G. Rumbles, Nature Mater. **5**, 683 (2006).
[16] G. P. Wiederrecht, G. A. Wurtz, and J. Hranisavljevic, Nano Lett. **4**, 2121 (2004).
[17] P. Walczak, A. Eisfeld, and J. S. Briggs, J. Chem. Phys. **128**, 044505 (2008).
[18] M. Wewer and F. Stienkemeier, J. Chem. Phys. **120**, 1239 (2004).
[19] M. Schreiber and Y. Toyozawa, J. Phys. Soc. Jpn. **51**, 1528 (1982).
[20] H. Fidder, J. Knoester, and D. A. Wiersma, J. Chem. Phys. **95**, 7880 (1991).
[21] C. Didraga and J. Knoester, J. Chem. Phys. **121**, 10687 (2004).
[22] P. Heřman, U. Kleinekathöfer, I. Barvik, and M. Schreiber, Chem. Phys. **275**, 1 (2002).
[23] E. W. Knapp, Chem. Phys. **85**, 73 (1984).
[24] V. A. Malyshev, J. Lumin. **55**, 225 (1993).
[25] A. V. Malyshev, V. A. Malyshev, and F. Dominguez-Adame, J. Phys. Chem. B **107**, 4418 (2003).
[26] V. A. Malyshev, A. Rodriguez, and F. Dominguez-Adame, Phys. Rev. B **60**, 14140 (1999).
[27] M. Bednarz, V. A. Malyshev, and J. Knoester, Phys. Rev. Lett. **91**, 217401 (2003).
[28] M. Bednarz, V. A. Malyshev, and J. Knoester, J. Chem. Phys. **120**, 3827 (2004).
[29] E. S. Medvedev and V. I. Osherov, *Radiationless Transitions in Polyatomic Molecules*, Springer Series in Chemical Physics Vol. 57 (Springer-Verlag, Berlin, 1995).
[30] R. Schinke, *Photodissociation Dynamics* (Cambridge University Press, Cambridge, 1995).
[31] S. Koller, J. Seibt, P. Marquetand, and V. Engel, Chem. Phys. Lett. **433**, 199 (2006).
[32] J. S. Briggs and A. Herzenberg, Mol. Phys. **21**, 865 (1971).
[33] A. Eisfeld and J. S. Briggs, Chem. Phys. **281**, 61 (2002).
[34] A. Eisfeld and J. S. Briggs, Phys. Rev. Lett. **96**, 113003 (2006).
[35] A. Eisfeld and J. S. Briggs, Chem. Phys. **324**, 376 (2006).
[36] A. Eisfeld, R. Kniprath, and J. Briggs, J. Chem. Phys. **126**, 104904 (2007).
[37] A. Eisfeld and J. S. Briggs, Chem. Phys. Lett. **446**, 354 (2007).
[38] W. T. Simpson and D. L. Peterson, J. Chem. Phys. **26**, 588 (1957).
[39] R. E. Merrifield, J. Chem. Phys. **28**, 647 (1958).
[40] A. Bierman, J. Chem. Phys. **46**, 2124 (1967).
[41] J. L. Magee and K. Funabashi, J. Chem. Phys. **34**, 1715 (1961).
[42] J. Roden, A. Eisfeld, and J. S. Briggs, Chem. Phys. **352**, 258 (2008).
[43] B. Kopainsky, J. K. Hallermeier, and W. Kaiser, Chem. Phys. Lett. **83**, 498 (1981).
[44] A. Eisfeld, L. Braun, W. T. Strunz, J. S. Briggs, J. Beck, and V. Engel, J. Chem. Phys. **122**, 134103 (2005).
[45] M. Hoffmann, K. Schmidt, T. Fritz, T. Hasche, V. M. Agranovich, and K. Leo, Chem. Phys. **258**, 73 (2000).
[46] S. Kirstein and S. Dähne, Int. J. Photoenergy **2006**, 20363 (2006).
[47] D. Möbius and H. Kuhn, J. Appl. Phys. **64**, 5138 (1988).
[48] S. S. Lampoura, C. Spitz, S. Dähne, J. Knoester, and K. Duppen, J. Phys. Chem. B **106**, 3103 (2002).
[49] V. I. Prokhorenko, D. B. Steensgaard, and A. R. Holzwarth, Biophys. J. **85**, 3173 (2003).
[50] J. S. Briggs, Ph.D. thesis, Victoria University of Manchester, 1968.